

STOCHASTIC FEATURES OF MULTIPACTOR IN COAXIAL WAVEGUIDES FOR TRAVELLING AND STANDING WAVES*

Gennady Romanov[#], Fermilab, Batavia, IL 60510, USA.

Abstract

CST Particle Studio combines electromagnetic field simulation, multi-particle tracking, adequate post-processing and advanced probabilistic emission model, which is the most important new capability in multipactor simulation. The emission model includes in simulation the stochastic properties of emission and adds primary electron elastic and inelastic reflection from the surfaces. The simulation of multipactor in coaxial waveguides have been performed to study the effects of the innovations on the multipactor threshold and the range over which multipactor can occur. The results compared with available previous experiments and simulations as well as the technique of MP simulation with CST PS are presented and discussed.

INTRODUCTION

Secondary electron emission RF discharge or multipactor was studied since early 1930's [1]. As a rule it is a serious obstacle to be avoided for normal operation of particle accelerator and their RF components. Theoretical studies of the multipactor phenomenon have to a great extent been performed using a one-dimensional model with a spatially uniform approximation of the electromagnetic field. However, many common RF devices involve structures where the field is inhomogeneous, and breakdown predictions based on such simple models will not be reliable. A numerical simulation of multipactor became an essential tool to predict the multipactor regions even for devices of simple geometries. Often these predictions are not in a full agreement with the experiments where the multipactor was observed. An important reason for this discrepancy is that some of the factors of complicated multipactor phenomena are not taken into account in the models.

MULTIPACTOR MODELS AND CODES

There are a number of numerical simulation codes for predicting multipactor each with various pros and cons. Many of these simulation codes are 1D and 2D and use the semi-empirical approach derived by Vaughan [2] to determine secondary emission. In essence the model assumes that all electrons leaving the material do so with an energy distribution commensurate with that of a secondary electron, hence electron reflection is not accounted for. Although some approaches have been developed that incorporate electron reflection to study multipactor [3,4], they have been quite limited in application.

Also many codes use macroparticles instead of individual electrons, where the macroparticle represents a large number of electrons all located at the same point, with identical momentum. The use of macroparticles means that information about the energy distribution cannot accurately be resolved and the statistical nature of electron reflection and emission is at best integrated over and effectively smoothed out. In many cases it is a useful assumption to make, but this algorithm is very ineffective when the statistical distributions are not negligible. The importance of multiparticle approach has been recognized early, but only a few attempts were made to develop a multiparticle model which would be closer to the real statistical nature of multipactor (see [4,5] for example). Tremendous programming and computing challenges limited such attempts until recently.

In general, the multipactor phenomenon is discussed in terms of resonance between the oscillations of the electrons and the RF electric field in the device volume. When resonance theory is used to analyze multipactor, it predicts growth of an electron avalanche only within relatively narrow separated bands of field levels. However, in the experiments the multipactor is observed mostly within a wider range of field levels with the overlapped (merged) multipactor zones. It was found that one important reason for this discrepancy is the spread of initial electron emission velocity, which results in a considerable spread of the corresponding flight times especially at higher multipactor modes. Therefore a part of the electron impacts at 'wrong' phases of the microwave field. But if the secondary emission is high enough a polyphase or non-resonant type of multipactor can arise giving the continuous distribution of multipactor as a function of input power close to that found in the experiments [6,7].

The paper [8] shows how the statistical nature of the combined factors described above can affect the multipacting behaviour of a RF structure in general. In this work Vaughan's standard model has been extended by using a Gaussian energy distribution for secondary electron energies and elastic/inelastic reflections with fixed probabilities. The model was used to study multipactor discharge between infinite parallel plates with separation of 1 mm. Although the model used in the paper was rather simplistic it was remarkably capable of the quantitative reproducing experimental results. The Hatch diagram in Fig.1 taken from [8] illustrates the main conclusion of the work that the inclusion of statistical factors broadens the multipactor bands and predicts the occurrence of multipactor well beyond "classic" model predictions.

*Work supported by US Department of Energy

[#]gromanov@fnal.gov

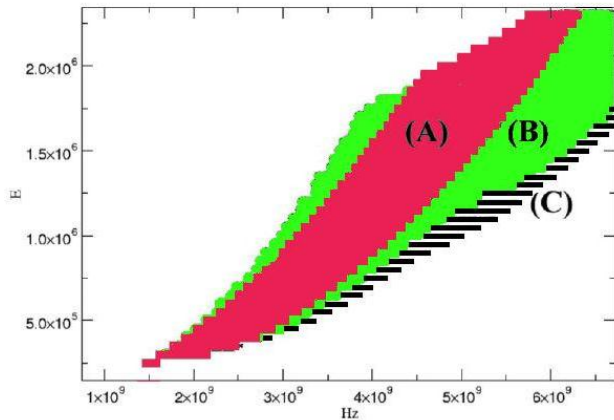


Fig. 1. Hatch diagram for parallel plate geometry, separated by 1 mm, that shows electric field (in V) magnitude versus frequency (in Hz), colored regions show where first-order multipactor will occur. The red band (A) represents the multipactor regions with no reflection and fixed secondary emission energy of 1 eV. Green band (B) represents the multipactor regions with no reflection and a Gaussian secondary energy distribution. Black bars (C) represent the multipactor regions with elastic/inelastic reflection with fixed probabilities and a Gaussian secondary energy distribution. Taken from [8].

Of course, for design and study of real RF accelerating cavities and RF components with their complex geometry and non-uniform electromagnetic fields, software that combines electromagnetic field simulation, multi-particle tracking, and advanced probabilistic emission model is needed. CST Studio Suit offers the code CST Particle Studio that is capable to perform multipactor study using either tracking solver or Particle-In-Cell solver. One of the important advantages of CST PS is the ability to include parameters that are stochastic in nature and to manipulate them by will. This ability is provided by advanced emission model. Recent work by Furman and Pivi as given in [9] has led to a probabilistic emission model that incorporates reflection, making the distinction between the different probabilities for secondary emission and inelastic and elastic scattering. The model is based on a broad phenomenological fit to data for the secondary-emission yield and the emitted-energy spectrum, which gives a very good fit to experimental secondary emission yield (SEY) data including dependence on impact angle. There are a number of user-defined parameters used by the Furman-Pivi algorithm, so practically any SEY configuration can be simulated.

In this paper the effects of stochastic properties of emission and the actual value of secondary emission on the multipactor threshold as well as on the existence of a discharge in a coaxial waveguide are considered. Such studies with some limitations and assumptions have previously been done [10,11,12 and elsewhere], but more powerful and sophisticated tool such as CST Particle Studio reveals more details.

There is another important effect that is present when electric field is spatially non-uniform. This is so called ponderomotive or Gaponov-Miller [13] force, which

tends to push charged particles towards regions of low field amplitude. This can have both a qualitative and a quantitative effect on the multipactor regions and definitely makes a difference for travelling and standing waves in coaxial waveguide. To predict how the Gaponov-Miller force will affect the multipactor threshold the simulations that include 3D electron dynamic are necessary. The result for multipactor threshold in case of standing wave in coaxial waveguide found in [14, 15] suggests that the Miller force had no significant influence on the multipactor threshold. This result has been considered somewhat surprising by the authors of [12]. Their doubt is absolutely reasonable in light of the effect of the Gaponov-Miller force. A series of simulations has been performed in this work in order to get better understanding what happens to the multipactor threshold in the case of a standing wave in coaxial waveguide.

MODEL USED AND SIMULATION TIPS

The 50 Ω coaxial waveguide with an outer diameter of 103 mm and inner diameter 44.8 mm used in the couplers for the SPL 704 MHz superconducting cavities was taken for modelling from [16] (Fig.2). It was chosen because the MP simulations in [16] were performed using different codes, and there are the results to compare with. Besides the medium energy superconducting part of H-accelerator for Fermilab's ProjectX [17] has close operating frequency of 650 MHz, so the modelling and simulation can be useful for that project as well.

The model is very simple and the general recommendations on MP simulations using CST PS can be found elsewhere [18,19,20]. Here only a few important additional tips are given.

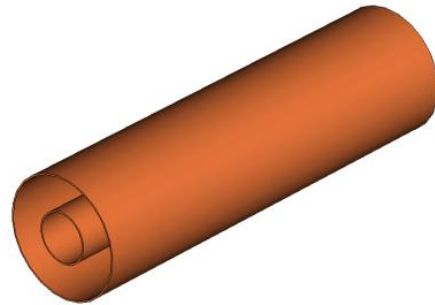


Fig.2. CST PS model of 50 Ω coaxial waveguide. Material of walls is annealed copper. Outer diameter is 103 mm and inner diameter is 44.8 mm, length is variable depending on task.

Particle sources and model solids

In complex RF devices multipactor can exist in different areas and hit different surfaces. Often the parts of a device are made of different materials. So, it is natural and convenient to have a model consisting of separate solids and place particle sources on separate surfaces in suspicious areas. First, it gives a freedom to change material properties of solids independently and perform simulation with single chosen particle source. Secondly, it allows analyzing collision data for each solid

and each particle source separately to define the most vulnerable surface in RF device.

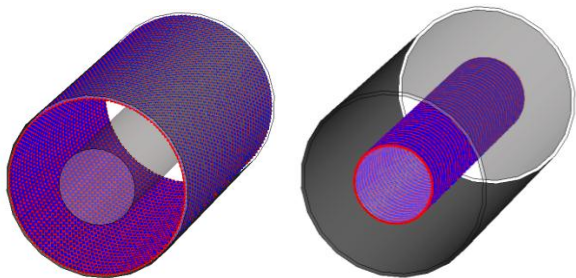


Fig.3. Sources of initial electrons in the model

In a simple coaxial waveguide considered in the paper, there are only two separate solids – outer and inner conductors. Each of these solids is assigned with separate source of initial electrons (see Fig.3). The electrons are uniformly distributed over the electrodes surfaces; they have initial energy uniformly distributed over 0-4 eV range and initial uniform angular spread $\pm 45^\circ$. Typical initial number of electrons was 3000-5000 for each source. Later the parameters of secondary and reflected electrons are governed by the Furman-Pivi emission model.

Travelling wave solution.

For particle tracking Particle Studio uses RF fields calculated by eigenmode solver only. Normally eigenmode solver gives a standing wave solution, while commonly travelling wave regime is required in waveguides. Fortunately the CST eigenmode solver has an option of setting phase advance at z-direction for periodic boundary conditions. If the periodic boundary conditions are set with arbitrary phase advance, the eigenmode solution is a travelling wave in general [19, 21]. An appropriate phase advance can be evaluated using equation:

$$f = \left[2(k - 1) \pm \frac{\Delta\varphi}{\pi} \right] \frac{c}{2L},$$

where f is a required frequency, L is a given waveguide length, $k = 1, \dots, n$. It is recommended to use this evaluation as a starting point and refine phase advance using optimization available in CST PS, since a result may be slightly different due to the numerical solving.

New CST Particle-In-Cell solver can use TW fields calculated in frequency domain or in time domain, so no manipulation with boundary conditions is needed. But in time of working on this paper a few results have been obtained with this solver yet.

Indication of MP

The simple diagnostic of MP in simulation is an integrated secondary emission yield or averaged secondary emission yield per impact $\langle \text{SEY} \rangle$ which can be calculated by dividing the total number of the secondary emitted electrons by the total number of hits

[18,19]. It is a convenient parameter, since it is easily calculated from CST PS output tables, and it is clearly correlated with SEY of material and average energy of impacts. Naturally, $\langle \text{SEY} \rangle$ more than unit indicates ongoing electron multiplication.

CST Particle Studio tutorial on multipactor simulation recommends exponential growth as an indicator of MP. But some of multipactor processes don't have an exponential growth of particles. For example, number of particles in multipactor on ceramic surface is regulated by floating potential on ceramic [22]. In this case a number of particles or multipactor current reaches saturation and generally speaking remains constant. Besides, as it will be shown below, we don't actually need to reach exponential growth of particles at all to evaluate multipactor power zones in RF device, which is a primary goal of the practical simulations.

Of course, both parameters only indicate a multipactor in simulations. They cannot predict severity of multipactor or its consequences: breakdown, detuning, mismatching etc. A new CST PIC solver can be used for such predictions, but discussion of the issue is beyond the scope of this paper.

Mesh density and number of initial particles

The issues of mesh density and number of initial electrons are very important because they directly affect accuracy and time of simulations.

A study of mesh density influence on simulation accuracy was done with 650 MHz coaxial waveguide ($Z=70 \Omega$, $D = 20.57 \text{ mm}$, $d = 6.35 \text{ mm}$). In this study the mesh density was varied, while the integrated $\langle \text{SEY} \rangle$ and the average impact energy $\langle E_i \rangle$ were calculated and recorded. RF field level corresponded to some resonant multipactor, emission properties were kept constant. Initial particles covered uniformly both outer and inner conductors, and in all runs the initial particles were emitted at the same phase with energy uniformly distributed over 0-4 eV. The total number of initial electrons was ≈ 3000 throughout the simulations. The result of the study is presented in Table 1.

Table 1

Number of mesh lines per wavelength	Meshcell number	$\langle \text{SEY} \rangle$	$\langle E_i \rangle, \text{eV}$
30	238208	1.817	519
35	375347	1.782	538
40	557032	1.81	537
45	763992	1.789	539
50	1047600	1.799	529
55	1479680	1.785	526
60	1911124	1.783	528
65	2419200	1.787	506
70	3010172	1.78	519

This extensive simulation has shown no visible dependence of multipactor parameters on mesh density: variation of $\langle \text{SEY} \rangle$ is $< \pm 1\%$ and variation of $\langle E_i \rangle$ is $< \pm 3\%$ through all mesh density values.

These results contradict the conclusion made in [19], that reliable multipactor prediction requires very high mesh density. Since that conclusion was made for a rectangular waveguide, the study with the same model of rectangular waveguide used in [19] has been done, but it did not confirm the conclusion either [23]. This disagreement is definitely due to too small number of initial particles used in those simulations – only 150 initial particles.

Using a small number of initial particles leads to a considerable stochastic fluctuation in the results which converge only with increasing accuracy of tracking in very fine fields. A sufficient large number of initial particles generates a tremendous number of hits and secondary particles (up to several millions). That makes the average values very consistent in spite of not very smooth fields calculated with a mesh of modest density. Of course, the mesh cells equal or bigger than the average electron trajectories are not acceptable.

If it is known where in a cavity and at what field level multipactor occurs, then a total number of initial particles can be significantly reduced, even only one correct particle can initiate multiplication process. But usually the multipactor parameters is exactly what we want to find out. Generally in search of multipactor zones a number of initial particles must be large even in case a previously performed field simulation that revealed suspicious spots. But actually a big number of initial particles is not a main problem, because most of them are lost during first several RF periods. It can be seen in Fig.5 that the number of particles initially drops, indicating the loss out-of-phase particles and then rapidly rises due to multipacting. A real problem for calculations begins when a multipactor occurs and an exponential (or close to) growth of particles starts.

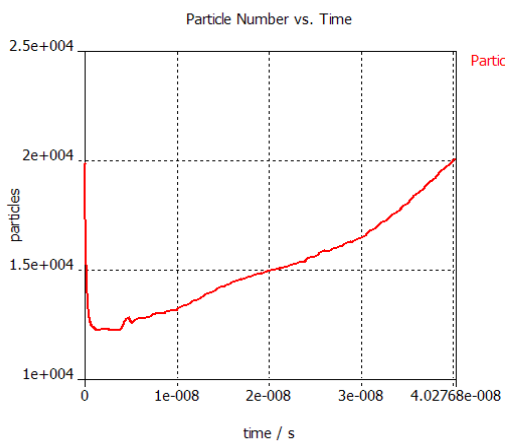


Fig.5. Initial drop and following growth of the number of particles.

On the other hand large number of initial particles allows avoiding extensive scanning of initial field phases.

In fact only one phase at which most initial particles can leave a surface and be captured in a process can be used. After number of RF periods the particles will be redistributed over phases and space in “optimal” way due to energy and velocity spread after multiple re-emissions (Fig.6 and 7).

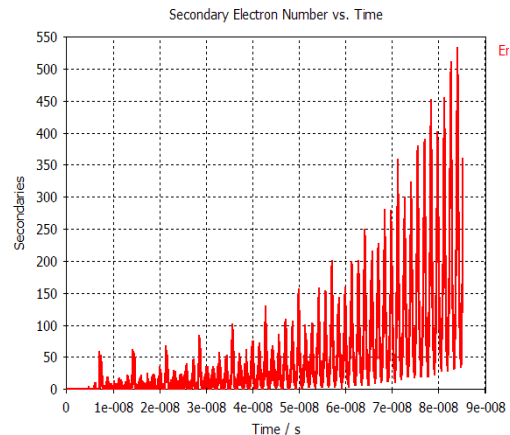


Fig.6. Secondary electrons gradually fill in all RF buckets.

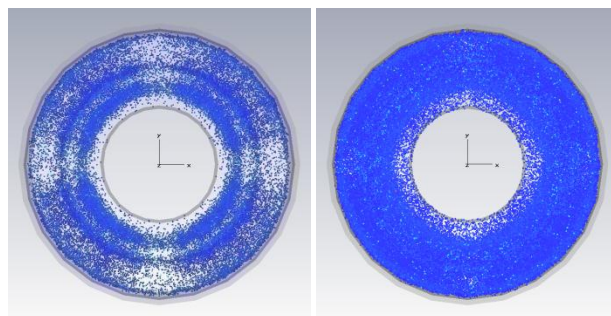


Fig.7. Spatial re-distribution of the electrons during simulation in the beginning (left) and in the developed stage (right).

Of course, large number of particles requires powerful computers and long simulation times. Unfortunately, this brutal force approach seems to be the most reliable way to simulate multipactor in real cases.

TW SIMULATION

Effect of probabilistic emission model

As it was mentioned above, some experimental observations such as a broad continuous range of multipactor instead of the narrow resonant bands, have been understood by taking into account spread of the initial electron velocity and elastic/inelastic reflections. But the models and codes used in these studies are far from being a universal powerful tool for multipactor simulation. Multiparticle simulations with advanced probabilistic emission model can include all aspects of the multipactor, which are difficult to analyze theoretically or using codes based on simplified models. This study was performed using CST PS to compare the simulation with the results of single-particle code RKpactor [16] and

study how prediction of multipactor threshold evolves with improving of emission model.

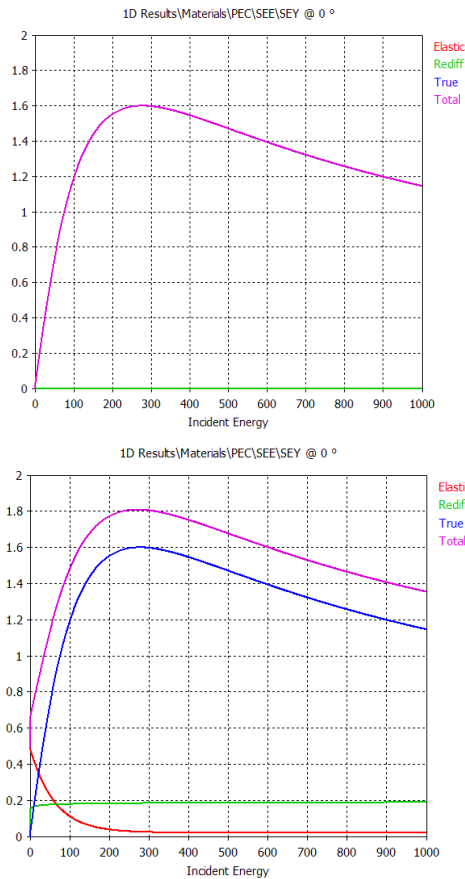


Fig.8. SEY functions used in CST PS simulations.

RKpactor code tracks one particle at a time and is optimized for identifying multipactor trajectories. The code uses the emission model taken from [4], but without elastic/inelastic reflections, since RKpactor is a single-particle code and cannot use complete distributed secondary emission model. A peak secondary emission yield of 1.6 was chosen for the simulations in [16]. Multipactor is identified in the code by the number of secondaries produced for a persistent (resonant) trajectory and growth of the electron current. If these reach user defined values a multipactor ‘event’ is recorded and the number of phases that give events is plotted versus power.

The first series of CST Particle Studio runs was performed with only true SEY function for copper without inelastic/elastic reflections to find agreement with RKpactor (see Fig.8, upper plot). But energy and angular spreads for true secondary electrons were in effect.

The second series of runs was performed using complete Furman-Pivi emission model for copper with SEY functions shown in Fig.8., bottom plot.

As can be seen in Figure 9, the results of first series show several distinct multipactor bands at various power levels, which are in excellent agreement with RKpactor results. But the bands in CST PS simulations are smeared and overlapped, especially at low power, due to the initial energy spread of secondary electrons.

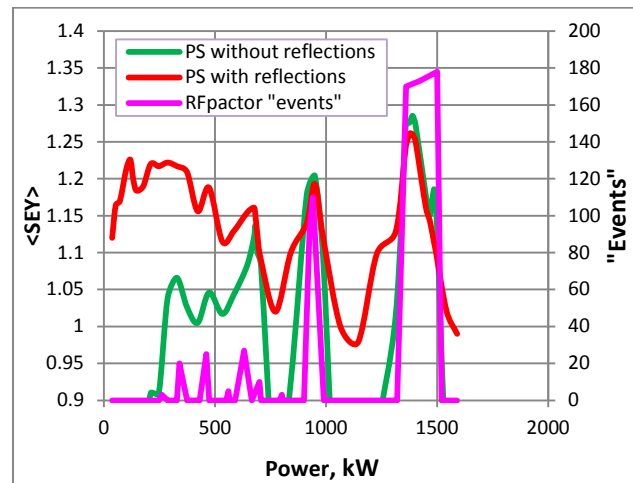


Fig.9. Comparison of CST PS and RKpactor simulations. CST PS is plotted against <SEY> and RFpactor is plotted against ‘events’ for various peak powers of electromagnetic wave.

The results of second CST series also show the same multipactor bands above 500 kW, though they are merged even stronger. Additionally the results show a consistent multipactor below 500 kW with a curve similar to the SEY curve. This does not appear in the RKpactor results and in first series of CST PS simulations, therefore this expansion of multipactor zone is due to the inclusion of elastic/inelastic electron reflection.

It is difficult to analyze and identify the character of multipacting through the whole power range, because actually it is a variable mix of one-side and two-side resonant and non-resonant trajectories. Fig.10 shows typical instant picture of the trajectories of particles that present at the given moment of time (“uncrushed particles”).

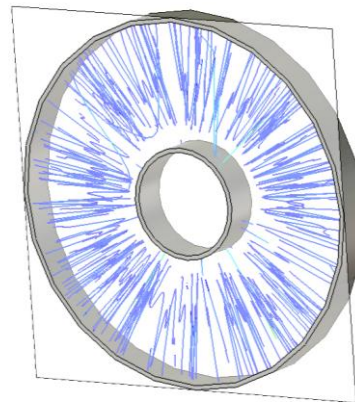


Fig.10. Slice of the coaxial waveguide with a snapshot of the “uncrushed particle” trajectories.

In general low power multipactor is largely non-resonant, while high power bands are the resonant ones. The difference in phase spread of secondary electrons for both cases can be seen in Fig.11.

So, both codes show the same results for the multipactor bands at high power, where the mass of trajectories are resonant. But for lower power end the single-particle

codes do not find sufficient number of resonant trajectories to indicate multipactor.

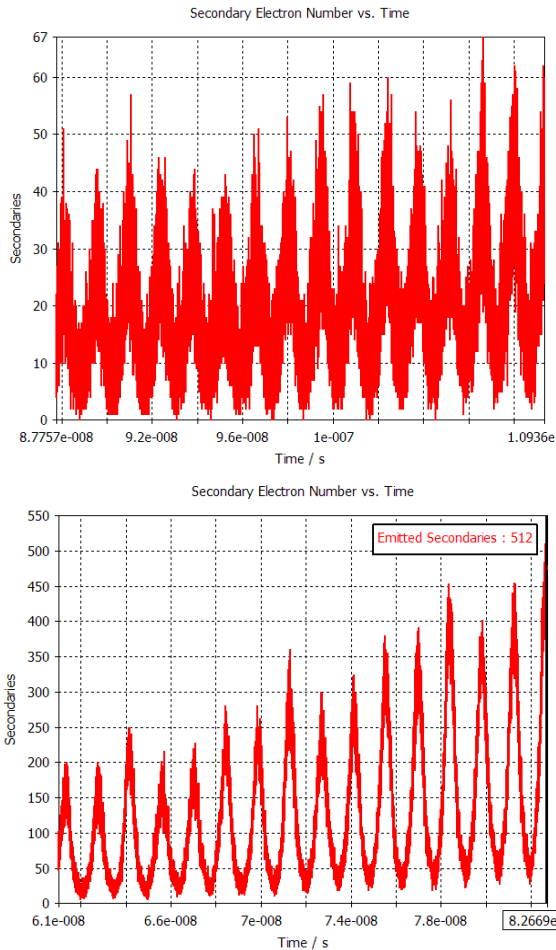


Fig.11. Secondary electron number vs time for non-resonant multipactor at 145 kW and resonant one at 950 kW of peak power.

This study has confirmed that the inclusion of probabilistic electron reflection and secondary electron velocity distribution leads to the overlapping of the multipacting zones and broadens the range over which multipactor can exist. The theory behind this phenomenon has been discussed in detail by several authors [4,6,7,8,10-12].

Search of multipactor with reduced emission

Multiparticle simulations with CST Particle Studio can take hours per one run depending on mesh density, initial number of electrons and particularly on true secondary electron emission yield, since this parameter defines the multiplication rate and total number of secondary particles. Usually for multipactor simulations a SEY function is taken from experimental results for given material. But in reality exact SEY value for material used in RF device is not known, because a condition of the material surface is unpredictable, and it is not necessarily the same as it was in the special experiments. Besides as a

rule a SEY value changes dramatically during RF conditioning.

As a matter of fact a practical goal of multipactor simulations during RF design is a search of potentially dangerous field level zones and locations inside RF device, rather than study of multipactor dynamic. In this sense the only reason for choosing high SEY value is a desire not to miss electron multiplication and therefore a multipactor zone. But this is a reasonable choice only if the exponential increase of secondary electrons is used for multipactor detection.

An average impact energy being independent on material and its SEY function could be a universal parameter to detect multipactor. But in CST Particle Studio it includes high energy impacts from diffused and elastically reflected electrons; therefore it is not accurate to estimate multiplication using arbitrary true SEY function. More convenient parameter for that is average secondary emission $\langle \text{SEY} \rangle$, defined earlier. Since it depends on given SEY, it characterizes a true multiplication.

Average $\langle \text{SEY} \rangle$ as a function of RF power has very important property – a similarity in respect to peak secondary emission of material. It means that if a true SEY peak value is changed as shown in Fig.12, then the $\langle \text{SEY} \rangle$ changes as shown in Fig.13.

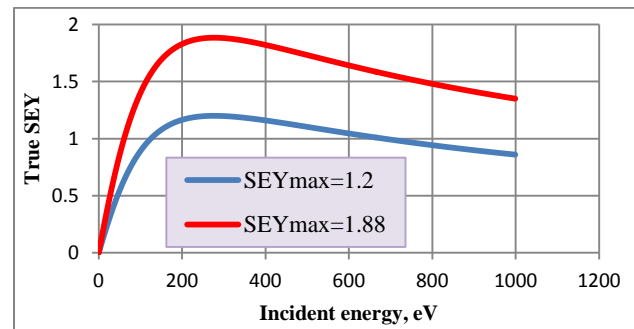


Fig.12. True SEY functions for copper in Furman-Pivi emission model for different peak SEY values.

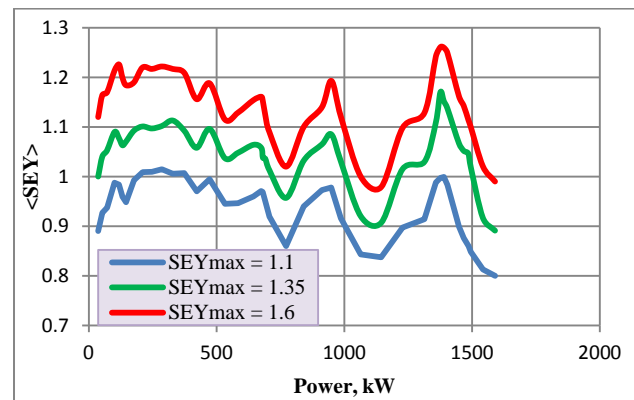


Fig.13. Average $\langle \text{SEY} \rangle$ as a function of power for different peak SEY values of material

The similarity is not absolute and the rise of the $\langle \text{SEY} \rangle$ is not proportional to the change of SEY peak value, because an interval of impact energies, where $\text{SEY} > 1$,

also changes. But the potential multipactor zone is the same for each curve with accuracy sufficient for practical purposes.

Now the $\langle \text{SEY} \rangle$ as a function of power can be found at low values of peak SEY. Then a potential multipactor zone can be defined without exponential multiplication of secondary particles. To get the reliable results a statistically sufficient number of impacts should be provided. It means that the number of initial electrons should be big enough, and that the peak SEY should be high enough to keep $\langle \text{SEY} \rangle$ around unit or slightly below. Then the number of electrons drops slowly (or even slightly increases) providing statistically sound number of impacts.

Because of lower emission the total number of particles used in such simulations is smaller by orders than that generated during an exponential increase of secondary electrons. It saves memory and reduces simulation time from several hours to several tens of minutes per run. Many of the simulation runs made for this paper have been finished only by virtue of this trick.

SW SIMULATION

Usually previous studies of multipactor in coaxial waveguides have been limited to the case of one dimensional electron motion along the radial direction of a waveguide. In case of travelling wave the field amplitude is constant along the waveguide, so there is no longitudinal Gaponov-Miller force, and thus the one-dimensional model is reliable also in the 3D case [12]. In a real waveguide, however, the field amplitude often varies due to mismatching, which gives rise to a standing wave pattern. In a number of cases a standing wave is a nominal operating field distribution in coaxial waveguides. In this paper only standing wave regime will be considered.

In SW case the electric field amplitude has sinusoidal distribution and changes from zero to maximum (see Fig.14). This implies a field gradient from field maxima to field minima. Due to the effect of the Gaponov-Miller force the electrons move along the waveguide towards the regions of lower field strength and get trapped into electric field node area.

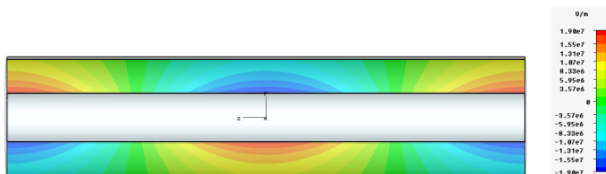


Fig.14. Standing wave electric field distribution

The effect of the Gaponov-Miller force was studied for mixed and standing waves in [24]. It was concluded that the multipactor threshold values strongly depend on the considered wave configuration, and the correlation between TW and SW thresholds is not that simple, contra to the results of [14,15].

Also an important conclusion has been made in [24], that the multipactor can be mitigated for the SW

configuration, due to the attractor effect of the nodes of the SW pattern. It has been analysed numerically and confirmed in the experiment (see Fig.14).

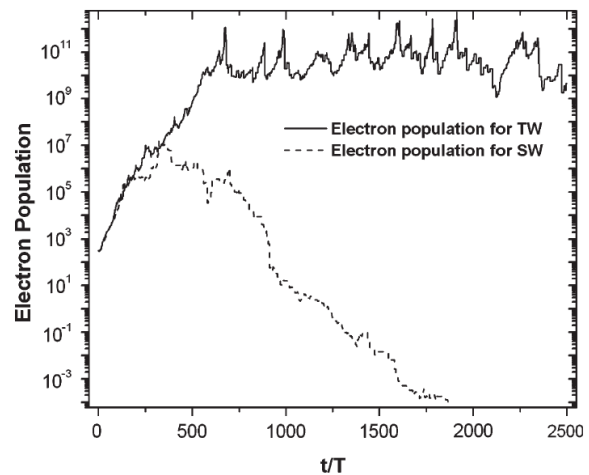


Fig.14. The evolution of the electron population in a coaxial transmission line of $Z_0 = 50 \Omega$, with a gap $d = 20 \text{ mm}$ and at $f = 0.75 \text{ GHz}$, for TW and SW. For both measurements the voltage was 2 kV. Taken from [24].

In this experiment the electron population for TW reaches some saturation level, determined by space charge effect. The electron population for SW increases just after RF power is on, while the electrons are still distributed more or less evenly over the waveguide. Then more and more secondary electrons drift toward null electric field, and the multipactor discharge is extinguished.

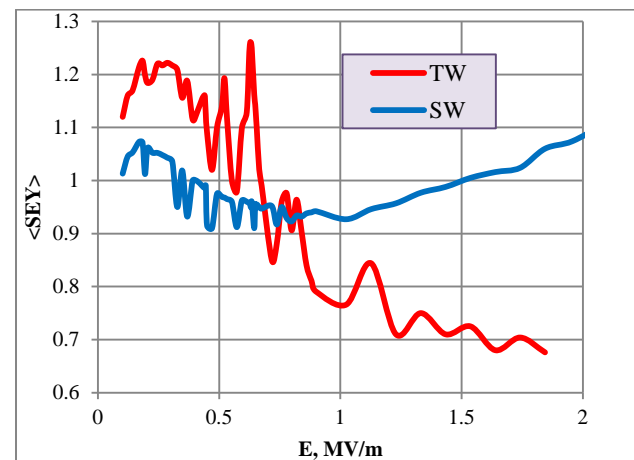


Fig.15. Average $\langle \text{SEY} \rangle$ versus electric field amplitude on the surface of inner electrode for TW and SW.

The detailed CST PS simulations performed for the chosen coaxial waveguide model and peak $\text{SEY} = 1.6$, confirmed this conclusion. But at the same time the simulation revealed in fact three different zones for multipactor in SW mode. These zones can be seen in Fig.15, where $\langle \text{SEY} \rangle$ for both TW and SW are plotted versus RF electric field amplitude on the surface of the inner electrode, which is more appropriate parameter than the voltage between electrodes or RF power.

For low electric field (up to 0.3 MV/m) the CW multipactor exists, and it is similar to non-resonant multipactor for TW case. Angular, velocity and energy spread of true secondary electrons along with high energy of the reflected electrons overcome the Gaponov–Miller force, which is not yet strong. So, there are enough electrons between the electric field nodes to support the discharge. For SW the behavior of the $\langle \text{SEY} \rangle$ function for the low field reminds that for TW, though the absolute value of the $\langle \text{SEY} \rangle$ for SW is much lower, because many secondary electrons are nevertheless lost at the electric field nodes. The instant picture of the low field steady-state CW multipactor is shown in Fig.16.

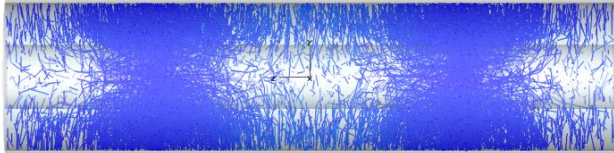


Fig.16. The snap-shot of the multipactor in standing wave for low electric field amplitude. The attraction effect of the Gaponov-Miller force is clearly seen.

In the medium field zone (0.3÷0.7 MV/m) the Gaponov-Miller force gains strength and all secondary electrons are eventually concentrated at the electric field nodes (Fig.17). There they cannot get a sufficient acceleration in this low field area and the discharge dies. The evolution of the simulated electron population for this case repeats the experimental curve from [24] (see Fig.18).

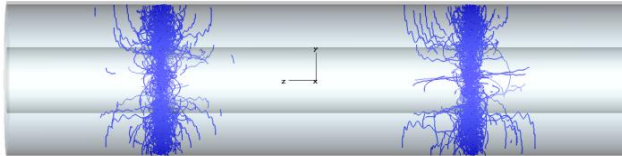


Fig.17. The snap-shot of the multipactor in standing wave for a medium electric field amplitude. The electron migration toward the field nodes is complete and the discharge is dying.

For electric field amplitudes above 0.7 MV/m the concentration of electrons becomes even denser (Fig.19), but surprisingly enough the multipactor discharge restores. One can speculate about two reasons for that. First, the electrons oscillate around zero electric field nodes with amplitude, which remains finite even for very high electric field amplitude. In some sense it seems to be a consequence of the stochastic nature of the re-emission process, because the multipactor develops only with elastic/inelastic reflections on. But exact mechanism for that still should be understood better. Second, the electric field in the interval of electron oscillations becomes high enough to initiate re-emission process.

The Fig.20 shows $\langle \text{SEY} \rangle$ function over entire SW multipactor zone for different maximal values of SEY function. The similar shapes of $\langle \text{SEY} \rangle$ curves suggest that the simulations with low SEY can be used in search

of multipactor zones for SW regime as well as for TW one. The curves do not show any resonances and are very smooth, which means that the multipactor is non-resonant and stochastic through the complete multipactor zone.

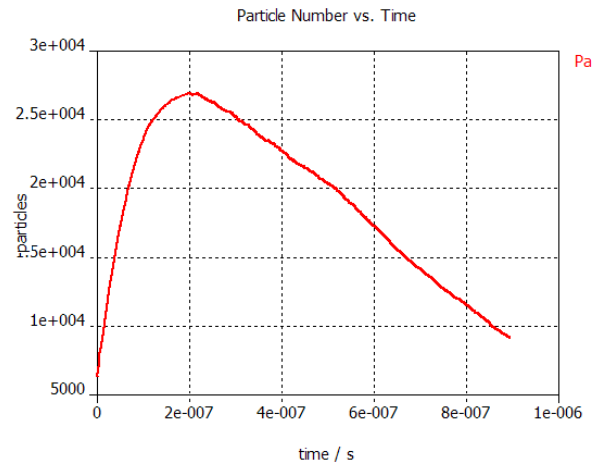


Fig.18. The simulated evolution of the electron population for a medium electric field amplitude.

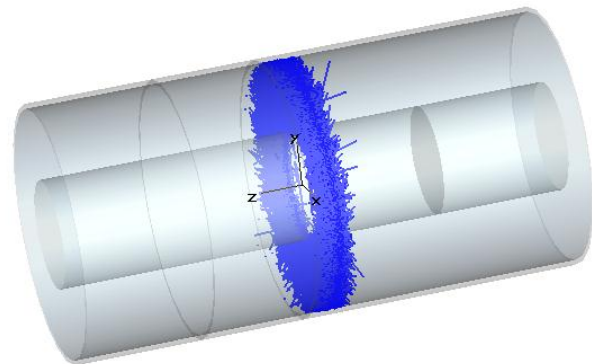


Fig.19. The snap-shot of the multipactor in standing wave for the electric field amplitude above 0.7 MV/m.

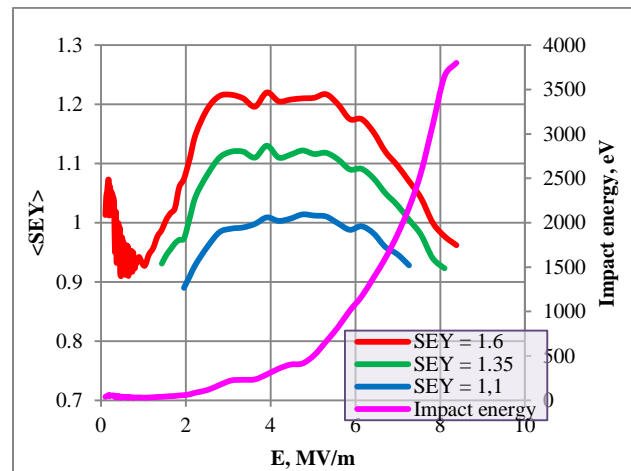


Fig.20. Average $\langle \text{SEY} \rangle$ for different peak SEY values of material and average impact energy versus electric field amplitude on the surface of inner electrode SW.

Also average impact energy versus field level is shown on the same plot. The $\langle \text{SEY} \rangle$ exceeds 1 when the average

energy of the impacts are between the crossover points of given SEY function.

In the simulations the multipactor at high field amplitudes is rather stable and persistent. But because of very small volume, where the discharge develops, the multipactor may be not very powerful in real coaxial devices.

CONCLUSION

Simulations of electron multipactor discharge in the coaxial waveguide have been performed using CST Particle Studio, with a primary goal to verify the effect of multi-particle approach combined with advanced probabilistic emission model on the discharge thresholds. Most simulations agree with analytical results and the results from more simplified numerical codes. It was confirmed and illustrated in details how incorporating an advanced emission broaden and merge the multipactor zones.

It was also confirmed that the multipactor for CW mode can be mitigated due to the effect of the Gaponov-Miller force. In addition to that it was found that at the electromagnetic field levels much higher than usual threshold for TW the multipactor can exist in the vicinity of the electric field nodes.

REFERENCES

- [1] P.T. Farnsworth, "Television by Electron Image Scanning", Journal of the Franklin Institute, vol.2, p.411, 1934
- [2] J. R. M. Vaughan, IEEE Trans. Electron Devices **35**, 1172, 1988.
- [3] V. Chernin, A. Drobot, and M. Kress, "A model of secondary emission for use in computer simulation of vacuum electronic devices," IEDM Tech. Dig., vol. 5, pp. 773–776, 1993.
- [4] V.P. Gopinath, J.P. Verboncoeur, and C.K. Birdsall, "Multipactor electron discharge physics using an improved secondary emission model," Phys. Plasmas, vol. 5, pp. 1535–1541, 1998.
- [5] L.V.Kravchuk et al "Mutipactoring Code for 3D Accelerating Structures", Proc. of Linac2000 Conf., Monterey, California, USA, 2000.
- [6] Grishin L.V., Dorofeyuk A.A., Kossyi I.A., Luk'yanchikov G.S. and Savchenko M.M., "A Study of Secondary-Emission Microwave Discharges with Large Electron Transit Angles", Lebedev Physics Institute Series vol 92, New York: Consultants Bureau, pp 63–101, 1977
- [7] Grishin L.V. and Luk'yanchikov G.S., "Multipactor discharge with an electron velocity distribution", Sov. Phys. Tech. Phys. **21** 307–11, 1976
- [8] R. Seviour, "The Role of Elastic and Inelastic Reflection in Multipactor Discharges", IEEE Trans. on Electron Devices, vol.54, No 8, August 2005
- [9] M.A. Furman and M.T.F. Pivi. "Probabilistic model for the simulation of secondary electron emission", Physical Review Special Topics, Accelerators and Beams, Volume 5. 2002.
- [10] A. Sazontov et al, "Effect of emission velocity spread of secondary electrons in two-sided multipactor", Phys. Plasmas, **12** 053102, 2005
- [11] V.E. Semenov et al, "Multipactor in a coaxial transmission line. II. Particle-in-cell simulations", Phys. Plasmas, **14**, 033509, 2007
- [12] R. Udiljak et al, "Multipactor in a coaxial transmission line. I. Analytical study", Phys. Plasmas **14**, 033508, 2007
- [13] A.V. Gaponov, M.A. Miller, "Potential Wells for Charged Particles in a High-Frequency Electromagnetic Field," Sov. Phys. JETP **7** (1958) 168.
- [14] E. Somersalo, P. Yla-Oijala, and D. Proch, in Proceedings of the 1995 Particle Accelerator Conference, Dallas, Texas, IEEE Conference Proceedings, Piscataway, NJ, p. 1500, 1996
- [15] E. Somersalo, P. Yla-Oijala, D. Proch, and J. Sarvas, Part. Accel. **59**, 107, 1998
- [16] G Burt et al, "Multipactor Simulations of the SPL Power Coupler", Proc. of LINAC10 conf., Tsukuba, Japan, 2010
- [17] N.Solyak et al, "The Concept Design of the CW Linac of the Project-X", Proc. IPAC10 conf., Kyoto, Japan, 2010
- [18] G.Romanov, "Simulation of Multipacting in HINS Accelerating Structures with CST Particle Studio", Proc. of LINAC08 Conf., Victoria, Canada
- [19] G.Burt et al, "Benchmarking Simulation of Multipactor in Rectangular Waveguides Using CST Particle Studio", Proc. of SRF2009 Conf., Berlin, Germany.
- [20] F. Hamme, U. Becker and P. Hammes, "Simulation of Secondary Electron Emission with CST Particle Studio_{tm}" Proceedings of ICAP 2006, Chamonix, France
- [21] Jiaru Shi et al, "Experiment on the Cold Test Model of a 2-Cell Superconducting Deflecting Cavity for ALS at LBNL", Proc. of PAC07, Albuquerque, New Mexico, USA
- [22] I.Gonin et al, "A Study of Multipactor Phenomena in the 52 MHz PETRA II Cavity at DESY", Proc. of EPAC94, London, Great Britain, 1994
- [23] Sergey Kazakov, private communication.
- [24] Antonio M. Perez et al, "Prediction of Multipactor Breakdown Threshold in Coaxial Transmission Lines for Travelling, Standing and Mixed Waves", IEEE Trans. on Plasma Science, vol.37, No 10, October 2009.